ACS OMEGA

http://pubs.acs.org/journal/acsodf

Article

Preparation of Manganese Oxide Nanoparticles with Enhanced Capacitive Properties Utilizing Gel Formation Method

Md. Abu Bakar Siddique, Ummey Hafsa Bithi, Aninda Nafis Ahmed, M. A. Gafur, Akter Hossain Reaz, Chanchal Kumar Roy, Md. Mominul Islam,* and Shakhawat H. Firoz*

Cite This: *ACS Omega* 2022, 7, 48007−48017

Read Online

ACCESS | Metrics & More | Article Recommendations | Supporting Information

ABSTRACT: Development of efficient and environmentally benign materials is important to satisfy the increasing demand for energy storage materials. Nanostructured transition-metal oxides are attractive because of their variety in morphology, high conductivity, and high theoretical capacitance. In this work, the nanostructured MnO_2 was successfully fabricated using a gel formation process followed by calcination at 400 °C (MNO4) and 700 °C (MNO7) in the presence of air. The suitability of the prepared materials for electrochemical capacitor application was investigated using graphite as an electrode substrate. The chemical, elemental, structural, morphological, and thermal characterizations of the materials were performed with relevant techniques. The structural and morphological analyses revealed to be a body-centered tetragonal crystal lattice with a nano-tablet-like porous surface. The capacitive performances of the MNO4- and MNO7-modified graphite electrodes were examined with cyclic voltammetry and chronopotentiometry in a 0.5 M Na_2SO_4 aqueous solution. The synthesized MNO7 demonstrated a higher specific capacitance (627.9 F g^{-1}), energy density (31.4 Wh kg^{-1}), and power density (803.5 W kg^{-1}) value as compared to that of MNO4. After 400 cycles, the material MNO7 preserves 100% of capacitance as its initial capacitance. The highly conductive network of nanotablet structure and porous morphologies of MNO7 are most likely responsible for its high capacitive behavior. Such material characteristics deserve a good candidate for electrode material in energy storage applications.

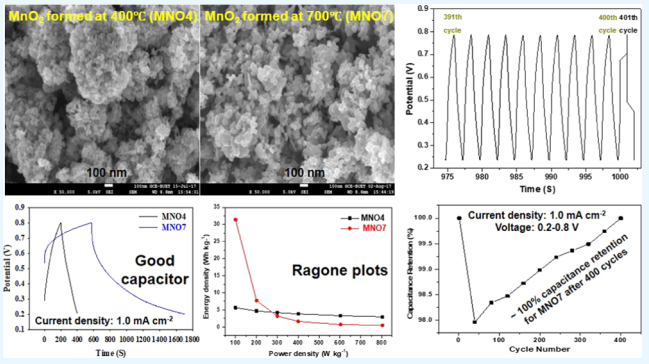

INTRODUCTION

The development of potential power sources to compete with ever-increasing energy demands is a significant worldwide issue.[1] With the growth of the market for portable electronic devices and hybrid electric vehicles, the need for energy storage devices is increasing.[2,3] Batteries, fuel cells, and supercapacitors are the most efficient and effective electrochemical energy conversion and storage technologies.[4−6] Due to various advantages, including environment-friendly, high power density, low cost, and so on, supercapacitors have attracted massive attention in recent research activities in the energy sector.[5−8] However, supercapacitors have a lower energy density than batteries, and hence increasing their energy density to that of batteries is desirable.[5,6] While the performances of supercapacitors are mainly determined by the electrode material rather than the construction mechanism, it is important to develop the most effective electrode materials from available sources using facile routes.[1,2]

Because of their high theoretical specific capacitance, nanostructured metal oxides of transition metals have been identified as viable electrode materials for supercapacitors recently.[1,5−7,9] Various metal oxides of transition metals, including oxides of manganese,[1,3,10,11] nickel,[12] iron,[13] and titanium,[14] have been reported for their potentiality as supercapacitor electrode materials. Even though ruthenium oxide has very high specific capacitance (720 F g^{-1}) and still performs electrochemically better as an electrode material, the high cost and toxicity of hydrous ruthenium oxide have limited its usage.[8,15] As a result, considerable efforts have been put into exploring possible low-cost and available electrode materials with good capacitive properties.

Manganese dioxide has attracted the interest of researchers because of its low cost, high theoretical capacitance (1370 F g^{-1}), reasonable lithium-storage capacities (615 mAh g^{-1} in lithium-ion batteries), low toxicity, variety of morphologies and allotropies, and excellent electrochemical capacitive performance in aqueous electrolytes via reversible and fast redox

Received: September 14, 2022
Accepted: November 30, 2022
Published: December 12, 2022

reactions near the exposed surface of the active materials.[6,7,16−18] To attain the advantage of theoretical specific capacitance of MnO_2, the material must have excellent ionic and electronic conductivities, stable nanostructure, and a large surface area, and improving these features for its supercapacitor applications is a crucial task.[2,8,9,19] Some efforts have been made to augment the surface area of MnO_2 in an attempt to enhance its electrochemical performance.[19−21] The significant variations in specific capacitance values can be observed in the reports. In fact, the diverse synthetic routes were followed by each research group, which crucially affect the chemical composition, crystallinity, morphology, particle size, surface area, porosity, and eventually the capacitive behavior.[9,22−24] The nanostructured electrode materials, which have large areas of exposed surface and can enlarge the surface to contact area, showed excellent electrochemical performance.[25] Hence, to achieve an optimized condition of the desired properties, MnO_2 with various morphologies, such as nanoflakes,[26] nanorods,[20,27] nanowires,[9,28] nanoworms,[29] nanopedals,[30] nanobelts,[21] nanoflowers,[8] urchin-like nanowhiskers,[31] and nanosheets,[32] has been developed. Additionally, the capacitance of MnO_2 is highly dependent on its surface morphology, which embraces lucid visualizations of crystallinity, particle size, surface area, and porosity of the material.[8]

In this regard, the synthesis pathway is vital in determining the morphology of MnO_2. Several routes for the synthesis of MnO_2 have been established including chemical coprecipitation,[33] hydrothermal,[34,35] thermal decomposition,[36] sol−gel,[37] electrochemical deposition,[11,24,38] and microwave-assisted hydrothermal[39] synthesis methods. Irrespective of synthesis procedures or morphologies of MnO_2, researchers employed commercial manganese-containing compounds such as Mn $(CH_3COO)_2$, $MnSO_4$, $KMnO_4$, and so on as precursors. Among the different synthesis methods, sol−gel is considered superior because it allows the formation of controlled morphology and is regarded as a highly versatile route for metal-oxide nanoparticle synthesis.[37,40] Even though the reaction and the chemistry inside the methods of gel formation by polyhydric alcohols are straightforward, however, significant research on the preparation of nanoparticles and their uses has not been well studied. It is anticipated that this method will enable uniform mixing of reactants on the molecular level, which may be utilized to control the morphology and particle size of the products. This is because the method is comparable to the conventional sol−gel process. Moreover, the preparation of MnO_2 by a gel formation synthetic route followed by calcination or heat treatment and its resulting electrochemical performance have not yet been reported. Reports have been found on the capacitive properties of MnO_2 prepared by different methods. For instance, Huang et al.[1] found a capacitive value of 400 F g^{-1} for MnO_2 synthesized by an electrochemical deposition technique, Xi et al.[20] found a value of 200 F g^{-1}, Wan et al.[25] synthesized MnO_2 by chemical precipitation method and obtained a capacitive value of 200 F g^{-1}, Ali et al.[8] developed a powdered nanoflower morphology of MnO_2 by electrowinning and obtained the capacitive value of 294 F g^{-1}, and Goikolea et al.[22] used polyol method to prepare MnO_2 and found capacitance equal to 130 F g^{-1}. All of the reported values are in the moderate range and still, there is an excellent opportunity to work with enhancing the capacitive performance of MnO_2 (1370 F g^{-1}).[7] As a result, it is essential to synthesize size and shape-controlled manganese oxide nanoparticles by following a gel formation route at room temperature, followed by calcination, and their evaluation of electrochemical properties along with structure and surface morphology.

Herein, a facile, efficient, and one-pot synthesis route for the preparation of MnO_2 was followed. The gel formed due to the reaction between potassium permanganate and glycerol followed by heat treatment advantageously assisted to achieve different morphologies of nanostructured MnO_2. The relevant analyses of the prepared materials were performed using Fourier transform-infrared (FT-IR), energy dispersive X-ray (EDX), X-ray diffraction (XRD), thermogravimetric (TG), and field emission scanning electron microscopic (FESEM) techniques. The possible candidacy of nanostructured MnO_2 as a supercapacitor was studied with cyclic voltammetric and chronopotentiometry methods in an aqueous Na_2SO_4 solution. The robustness of the prepared supercapacitor electrodes was investigated by continuous charging−discharging cycles.

EXPERIMENTAL SECTION

Materials and Reagents. The materials and reagents used in the experiment included potassium permanganate (Merck, India), glycerol (JHD, China), sulfuric acid (E. Merck, Germany), hydrochloric acid (RCI Lab-Scan, Thailand), polyvinyl alcohol (Merck, Germany), dimethyl sulfoxide (Lab-Scan, Ireland), and ethanol (Merck, Germany). The graphite rod (with a surface area of 0.30 cm^2) was purchased from Alfa Aesar; Analytical grade chemicals and reagents were purchased and utilized in the experiment as received without any further modification and purification. For aqueous solution preparation, the deionized water (DI) having a conductivity of less than 0.2 μS cm^{-1} and a resistance of 18.2 MΩ cm was obtained from an ultrapure water purification system (Barnstead nanopure, Model: D7031, Thermo Scientific) and was used throughout the whole experiment.

Synthesis of Materials. The redox reaction of glycerol and potassium permanganate ($KMnO_4$) in an aqueous solution resulted in the formation of MnO_2. A gel-type precursor was formed when 50 mL of 0.4 M aqueous glycerol solution was added dropwise into 100 mL of 0.3 M $KMnO_4$ aqueous solution under vigorous stirring for 20 min at room temperature (25 °C). The obtained gel was kept undisturbed for a period of 24 h. The resulting solid material was carefully washed with DI water and repeatedly centrifuged (Universal 16A, Hettich, Germany) several times (at 3000 rpm for 10 min) to remove excess K^+ ions. The product was then dried in a hot-air electric oven (DSO-500D, Digisystem, Taiwan) at 80 °C to get a blackish-brown-colored product. The obtained product was divided into two portions and annealed separately in an electric muffle furnace (LT 5/12, Nabertherm, Germany) under an air atmosphere for 6 h at two different temperatures of 400 and 700 °C.[40,41] The two different final products are named MNO4 and MNO7, respectively. The calcination temperature was chosen by the study of TG analysis, as shown in the Supplementary Information (SI) (Figure SF1a−c).

Characterization of the Materials. The X-ray diffractometer (model: D8 Advance, Bruker, Germany), usually operating at 40 kV and 40 mA with a radiation (λ = 1.5406 Å) of Cu Kα_1 and fitted with a scintillation detector, was used to record the XRD pattern of the prepared materials. The FT-IR spectrophotometer (model: FT-IR-8400, Shimadzu, Japan) was used to measure the FT-IR spectra of the materials on KBr pellets in the mid-IR region (4000−400 cm^{-1}). The morphology of the material's surface was visualized with a

https://doi.org/10.1021/acsomega.2c05872
ACS Omega 2022, 7, 48007−48017

Table 1. Elemental Composition and X-ray Crystallographic Data of the Synthesized Materials

	elemental composition from EDX analysis				X-ray crystallographic data					
							lattice parameters (Å)			
materials	sample location	Mn (atomic %)	O (atomic %)	tentative chemical formula	crystallite size (nm)	lattice strain	*a*	*b*	*c*	spacing (*d*)
MNO4	1	28.58	71.42	MnO_2	16.2	0.0069	9.85	9.85	2.79	3.11
	2	36.43	63.57							
	3	31.68	68.32							
	average	32.23	67.77							
MNO7	1	32.43	67.57	MnO_2	12.6	0.0116	9.86	9.86	2.97	3.12
	2	35.13	64.87							
	3	32.80	67.20							
	average	33.45	66.55							

Schottky FESEM (model: JSM-7600F, JEOL, Japan) fitted with an EDX detector that recorded spectra in the 0−10 kV range. A thermogravimetric analyzer (model: TG/DTA6300, Seiko Instruments Inc. EXSTAR6000, Japan) was used to perform thermogravimetric, differential thermogravimetric, and differential thermal analysis of the materials over a temperature range from ∼25 to 1000 °C in air and nitrogen atmospheres. The performance of the electrochemical behavior of the prepared materials was examined using cyclic voltammetry and chronopotentiometry in an electrochemical workstation (CHI-660E electrochemical analyzer, CH instruments).

Preparation of MnO_2-Modified Graphite Electrode. The synthesized MnO_2 was cast on a graphite disc electrode (surface area: 0.30 cm^2) by solvent casting and drop drying method.[42,43] Around 10−20 mg of the active material was disseminated in a mixture of ethanol and dimethyl sulfoxide (1:2.5) with the addition of polyvinyl alcohol (additive, 15% of the functional material weight). To make a homogeneous slurry, the mixture was sonicated for 30 min in an ultrasonic bath (UBT-1080, UNILAB). A micropipette was used to carefully drop 5−10 μL of the suspension over the previously dried, cleaned, and weighted graphite electrode surface, ensuring complete coverage of the exposed surface area of the electrode. The vacuum oven was then used to dry the prepared electrode at 50 °C. The overnight drying of the graphite electrode surface resulted in a thin coating. The amount of materials deposited on the electrode surface was in the range of 0.33−3.33 mg cm^{-2}. For the electrochemical study, these well-cast graphite electrodes were employed as the working electrode substrate.

Electrochemical Measurements. For the electrochemical experiments, a single-compartment three-electrode electrochemical cell with a rectangular platinum plate as a counter electrode, a Ag|AgCl|KCl (sat.) electrode as a reference electrode, and the modified graphite electrode as-fabricated above with an exposed surface area of ca. 0.30 cm^2 as the working electrode were employed. The electrochemical measurement was conducted in a freshly prepared aqueous electrolyte solution of 0.5 M Na_2SO_4.

The cyclic voltammetry of the samples was initially performed arbitrarily over several potential ranges and scan rates to find out the optimum potential window within which the materials demonstrated stable capacitive behavior corresponding to the symmetrical rectangular shape of the cyclic voltammogram (CV).[44,45] Then, the CVs were taken within a potential range of 0.2−0.8 V at different scan rates (mV s^{-1}) to retain the approximately symmetric rectangular shape of the CV corresponding to the capacitive behaviors.

To evaluate the specific capacitance (C_{sp}) of the synthesized materials, chronopotentiometry or galvanostatic charge−discharge (CD) measurements were performed at different current densities (mA cm^{-2}) within the suitable constant potential window (0.2−0.8 V) chosen from CV. From the CD curves of the prepared materials, the value of C_{sp} (F g^{-1}) was enumerated following eq 1[46,47]

$$C_{sp} = \frac{i\Delta t}{m\Delta E} \tag{1}$$

where i represents the discharge current (in ampere, A), Δt is the discharge time (in second, s), m represents the mass (in gram, g) of the active electrode material, and ΔE is the voltage (in volt, V).

Furthermore, electrochemical impedance spectroscopy (EIS) measurements were carried out in the frequency range of 0.1 Hz to 1 MHz with an AC amplitude of 5 mV in a 0.5 M Na_2SO_4 aqueous electrolyte. The energy density, E (Wh kg^{-1}), and power density, P (W kg^{-1}), of materials were also evaluated. The values of E and P for the synthesized materials were calculated from their respective CD curves using eqs 2 and 3, respectively[48,49]

$$E = \frac{0.5 \times C_{sp} \times (\Delta V)^2}{3.6} \tag{2}$$

$$P = \frac{E \times 3600}{\Delta t} \tag{3}$$

where ΔV is the potential window or range of operating voltage (in volt, V), and the other symbols have their meaning as defined above.

RESULTS AND DISCUSSION

Formation of Manganese Oxides via Sol−Gel. The formation of manganese oxide particles is taken place via a simple redox reaction between $KMnO_4$ and glycerol in an aqueous solution wherein the glycerol molecule is oxidized to CO_2 and water and, on the other hand, MnO_4^- ion is probably reduced to Mn_3O_4 through the following reaction[40,50]

$$6KMnO_4(aq) + C_3H_5(OH)_3(aq) \rightarrow 3K_2CO_3(aq) + 2Mn_3O_4(s) + 3CO_2(g) + 4H_2O \tag{4}$$

The reaction is forwarded through the gelation process involving the formation of a cross-linked network of manganese oxide sites and partially oxidized glycerol fragments and the condensation reaction of the so-formed gel producing

https://doi.org/10.1021/acsomega.2c05872
ACS Omega 2022, 7, 48007−48017

the precursors of the target product, manganese oxide.[40] Upon heat treatment at high temperatures, the neat form of manganese oxides has been reported to produce via an internal phase transition.[51,52] The final solid products, MNO4 and MNO7, obtained by heat treatment at 400 and 700 °C were characterized by various techniques, as systematically described below.

Elemental and Structural Analyses. The compositions of MNO4 and MNO7 were studied with EDX analysis. From the EDX results (SI, Figure SF1), the ratio of Mn/O of the materials was determined and summarized in Table 1. It is found that the ratio of Mn/O is determined to be 1:2 in both cases. Thus, the synthesized manganese oxides were MnO_2 in both cases. From XRD analysis (the patterns shown in Figure 1), both manganese oxide phases heat-treated at 400 and 700 °C were identified and confirmed as manganese (IV) oxide, MnO_2 (JCPDS Card No. 01-072-1982). The result confirmed that this is the α-MnO_2 isomer resembled with the structure of a body-centered tetragonal lattice (space group: $I4/m$ (87), lattice parameters a = 9.82 Å, b = 9.82 Å, and c = 2.85 Å). The diffraction peaks corresponding to 2θ values with crystal planes of 12.6° (110), 17.9° (200), 28.6° (130), 37.5° (211), 41.9° (301), 49.7° (141), 55.8° (600), 60.0° (251), and 69.3° (541) for both materials were consistent with the standard reference. No other extra/impurity diffraction peaks were detected in this XRD pattern. The MNO4 and MNO7 showed a high-intensity peak corresponding to 2θ values with crystal planes of 37.5° (211) and 28.62° (130), respectively, probably due to much time to diffract the X-ray beam. The interlayer spacing (d-spacing) and the crystallite size, along with the lattice strain of the prepared materials, were determined using Bragg's law and Scherrer's equation, respectively, from the corresponding high-intensity peak in the XRD pattern, by utilizing the Cu Kα wavelength of 1.5406 Å. Table 1 summarizes the crystallite size, lattice strain, lattice parameters, and d-spacing of the prepared MNO4 and MNO7. The calculated lattice parameters and the d-spacing of the prepared MnO_2 are well matched with the reference values reported in the JCPDS card (No. 01-072-1982). The synthesized MnO_2 is formed as a body-centered tetragonal crystal geometry.

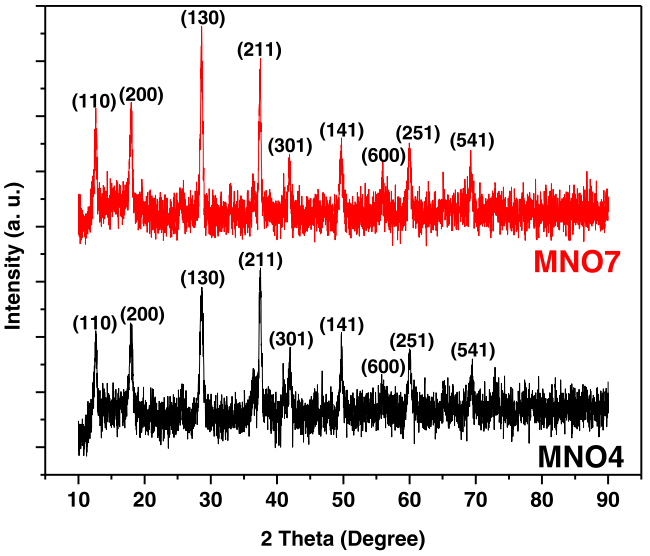

Figure 1. XRD patterns of manganese dioxide obtained at 400 °C (MNO4) and 700 °C (MNO7).

Chemical Characterization. The Mn−O bond and other inherent chemical functional groups in the samples were identified using FT-IR spectroscopic technique. Figure 2 represents the FT-IR spectra of the synthesized materials. The bands in the 400−750 cm^{-1} range can be attributed to distinctive stretching vibrations of O−Mn−O, confirming the existence of manganese oxide in samples.[53−55] The characteristic bands for MNO4 were found at 486, 537, 589, and 708 cm^{-1}, whereas those were found for MNO7 at 420, 535, 586, 670, and 709 cm^{-1}. These bands correspond to O−Mn−O stretching vibrations, indicating the presence of MnO_2 in the sample.[53−55] The broad band at 3438 cm^{-1} for MNO4 and 3442 cm^{-1} for MNO7 is associated with stretching vibrations of the adsorbed surface water molecule's hydrogen-bonded O−H group.[56] Furthermore, the narrow bands located at 1647 and 1385 cm^{-1} for MNO4 and 1646 cm^{-1} for MNO7 corroborated the existence of many residual O−H groups, indicating that the traces of adsorbed water vibrate in the O−H mode.[56] The stretching vibration of the C═O bond in the CO_2 molecule, which exploded while drying MnO_2 in connection with the CO_2 from the atmosphere, can be attributed to the weak sharp peaks at 2336 or 2338 and 2362 cm^{-1}.[57] The absorption peak for MNO4 at 1060 cm^{-1} represented the surface −OH groups of Mn−OH for colloidal MnO_2 nanoparticles.[53] The absence of absorption peaks near 1385 and 1060 cm^{-1} for MNO7 indicates that the sample contains fewer residual −OH groups and no surface −OH groups of Mn−OH for colloidal MnO_2 nanoparticles, respectively, as a result of heating at a relatively higher temperature (700 °C).[53] The findings of the FT-IR analysis presented here are consistent with those reported in the literature.[53−55] Overall, the FT-IR spectra are well supportive with structural analysis performed by XRD, confirming the formation of the desired materials.

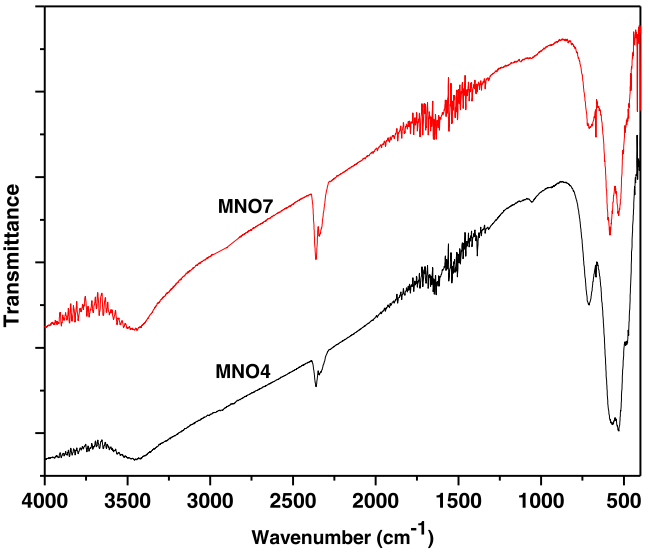

Figure 2. FT-IR spectra of the synthesized MNO4 and MNO7.

Thermal Analysis. Thermal stability and probable phase transformational behavior of MnO_2 were investigated with thermogravimetric (TG), differential thermogravimetric (DTG), and differential thermal analysis (DTA) techniques at temperatures ranging from 25 to 1000 °C under an

https://doi.org/10.1021/acsomega.2c05872
ACS Omega 2022, 7, 48007−48017

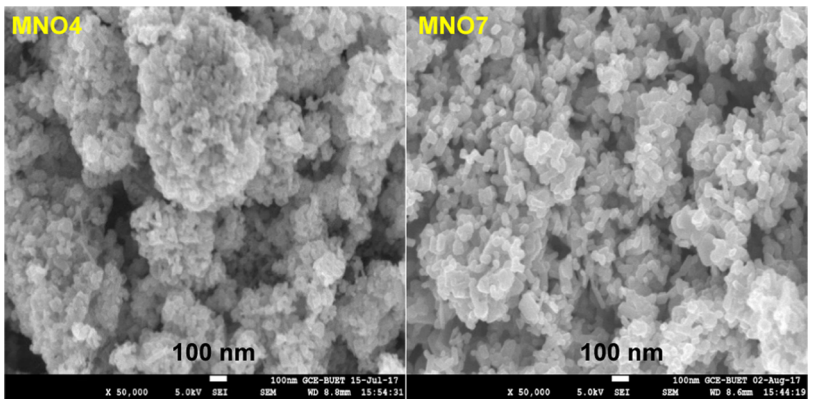

Figure 3. FESEM image of MnO_2 formed at 400 °C (MNO4) and 700 °C (MNO7).

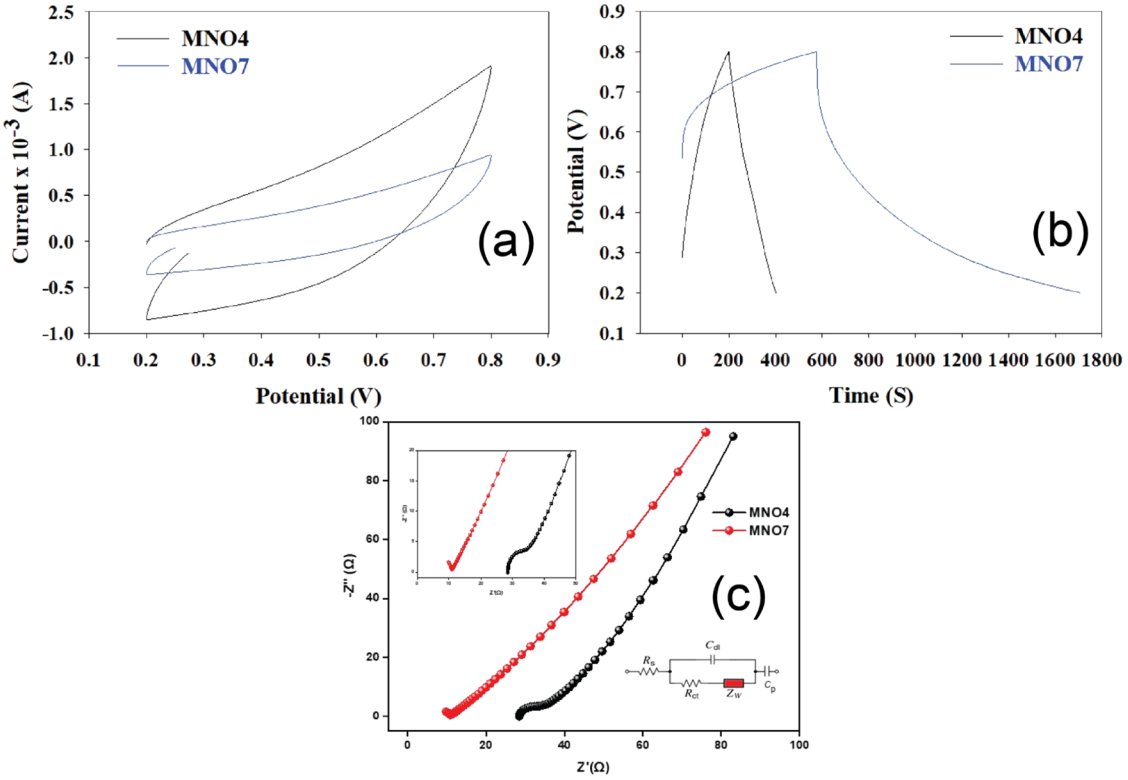

Figure 4. (a) Comparison of CVs of MNO4- and MNO7-modified graphite electrodes measured in 0.5 M Na_2SO_4 solution at a potential scan rate of 0.1 mV s^{-1}. (b) Comparison of CD curves of MNO4 and MNO7 measured at a current density of 0.1 mA cm^{-2}. (c) The corresponding Nyquist plots obtained for MNO4 and MNO7 along with the circuit fitted for evaluating different parameters.

atmosphere of air as well as nitrogen. These results are described in the SI along with Figure SF2a−c. The thermal analysis suggests that the changes in the phases and chemical composition in MNO7 calcined at 700 °C are negligible, whereas the dimerization of MnO_2 into Mn_2O_4 possibly took place in the case of MNO4 calcined at 400 °C.[58] However, both MNO4 and MNO7 have good thermal stability.

Study of Surface Morphology. The morphological examinations of MNO4 and MNO7 were performed using the FESEM technique, as represented in Figure 3. The FESEM image of MNO4 demonstrates a small and thick nanotablet (tablet in nanodimension) like particles of the material, which is highly aggregated and composed of various cluster groups. The prepared MNO4 appears to be comprised of randomly distributed spherical aggregates of nanoparticles (32.7 nm mean size) with distinct interparticle boundaries.

The surface morphology from the FESEM image of the MNO7 nanoparticle (Figure 3) shows less aggregation than that of the MNO4 nanoparticle during the high-temperature treatment. Particles of the small and thick tablet are more evident than that of MNO4 due to comparatively less aggregation of the nanoparticles. Moreover, a decrease in roughness and particle size was noticed for the sample treated at the elevated temperature. The approximate mean diameter of the MNO7 nanotablets is 28.3 nm, as estimated from the micrograph. The surface of MNO7 nanoparticles seems to be more highly porous than MNO4 and the particles are randomly distributed. A nanostructure of that kind of type could be expected to reduce the distance between ions as they diffuse in the solid phase.[55]

The disappearance of the agglomeration of particles resulting in a slight reduction of particle size due to the

https://doi.org/10.1021/acsomega.2c05872
ACS Omega 2022, 7, 48007−48017

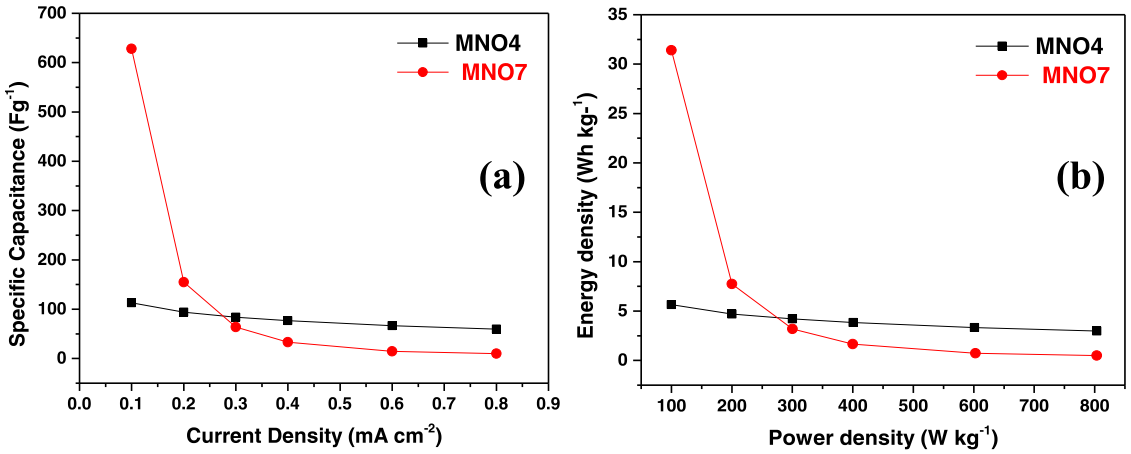

Figure 5. (a) Effects applying current density on specific capacitance and (b) Ragone plots.

Table 2. Comparison of the Capacitance Values of the Synthesized MnO_2 with the Literature

prepared method	nature of MnO_2	current collector	mass of electroactive material (mg cm^{-2})	electrolyte	measurement protocol	maximum capacitance (F g^{-1})	capacitance retention after cycle test	references
gel formation	powdered nanotablets	graphite rod	0.3	0.5 M Na_2SO_4	CP (I = 0.1 mA cm^{-2})	627.9	100% after 400 cycles	this work
electrochemical deposition	film	nickel foam	1.0	0.5 M K_2SO_4	CV (v = 5 mV s^{-1})	549		62
ultrashort pulsed electrochemical deposition	film	graphite substrate		ionic liquid gel polymer	CV (v = 10 mV s^{-1})	36.7		2
electrochemical deposition	film	nickel foam		0.5 M Na_2SO_4	CP (i = 1 A g^{-1})	400		1
electrochemical deposition	film	carbon cloth		1.0 M Na_2SO_4	CV (v = 5 mV s^{-1})	220	90% after 2500 cycles	20
electrochemical deposition	powdered nanobelts	stainless steel		1.0 M Na_2SO_4	CV (v = 25 mV s^{-1})	235.5	91.3% after 1000 cycles	23
hydrothermal	powdered nanorods	nickel foam		1.0 M Na_2SO_4	CV (v = 5 mV s^{-1})	102		26
chemical precipitation	powder	nickel foam	5	1.0 M Na_2SO_4	CV (v = 2 mV s^{-1})	452		25
electrowinning	powdered nanoflower	nickel foam	9.2	1.0 M Na_2SO_4	CP (i = 0.1 A g^{-1}) CV (v = 10 mV s^{-1})	294	~88% after 900 cycles	8
polyol method	powder	cavity microelectrode		0.1 M K_2SO_4	CV (v = 2 mV s^{-1})	130	~50% after 1 cycle (material loss)	22
hydrothermal	film	nickel foam	1.03	1.0 M Na_2SO_4	CP (i = 1 A g^{-1})	241	~90% after 1000 cycles	32

exposed higher temperature might be attributed to the use of glycerol in material synthesis. The reactions were forwarded through the gelation by cross-linked network formation of manganese oxide sites and partially oxidized glycerol fragments, which was followed by the condensation reaction of the gel to form manganese oxide.[40] The formation of a cross-linked network of manganese oxide sites probably leads to its agglomeration, which even persists greatly at a temperature of 400 °C, as evidenced by the FESEM image of MNO4 (Figure 3). The image indicates that the particles have a nonuniform size with a high degree of agglomeration. However, when this material is heat-treated at 700 °C, the cross-linked network with the glycerol fragments is broken down completely and the agglomeration of the particles disappears (Figure 3) leading to a slightly smaller size of the particles.

Electrochemical Capacitive Performance of the Materials. Figure 4a depicts the comparative CVs of the synthesized MnO_2 within the potential window of 0.2−0.8 V at a scan rate of 0.1 mV s^{-1}. Both CV curves showed an almost symmetrical rectangular shape demonstrating exemplary capacitance behavior. MNO7 shows a larger rectangular area of the CV than that produced by MNO4, indicating that MNO7 exhibits a higher capacitive behavior as compared to MNO4. CV curves were recorded by varying the potential scan rate to reveal more underlying information about the capacitance performance of the prepared nanostructured MnO_2 (SI, Figure SF3a,b). The variation of scan rate significantly influenced the CV curve shapes. The CV curve had a near-ideal shape of rectangular type at a slow scan rate, indicating that charging and discharging occurred at a constant rate across the applied voltage range.[59] The CV curves, on the other hand, deviate from the ideal rectangular shape, with an increasing scan rate.

Figure 4b shows the charge−discharge (CD) curve of MNO4 and MNO7 in the voltage range of 0.2−0.8 V

https://doi.org/10.1021/acsomega.2c05872
ACS Omega 2022, 7, 48007−48017

Table 3. Electrochemical Data of the Synthesized Materials

material	current density (mA cm $^{-2}$)	discharge time (s)	specific capacitance (F g^{-1})	energy density (Wh kg^{-1})	power density (W kg^{-1})
MNO4	0.1	203.7	113.2	5.66	100.0
	0.2	84.4	93.8	4.69	200.0
	0.3	50.3	83.9	4.20	300.2
	0.4	34.5	76.8	3.84	400.7
	0.6	19.9	66.5	3.33	601.5
	0.8	13.4	59.8	2.99	803.3
MNO7	0.1	1130.2	627.9	31.4	100.0
	0.2	139.3	154.8	7.74	200.0
	0.3	38.3	63.9	3.20	300.3
	0.4	14.8	32.9	1.65	400.1
	0.6	4.30	14.4	0.72	602.8
	0.8	2.20	9.82	0.49	803.5

measured by applying a current density of 0.1 mA cm^{-2}. The MNO7-modified graphite electrode showed a relatively higher discharging/charging time ratio (1.96) than that with MNO4 (1.03). This implies a considerably higher storage capacity of electric charge in the MNO7 electrode. The CD curves measured by applying different current densities are depicted in Figure SF4 (SI). The C_{sp} values for both MNO4 and MNO7 nanoparticles at different current densities are compared in Figure 5a. The C_{sp} of MNO7 nanoparticles decreased sharply with increasing current density. In contrast, the extent of the decrease in MNO4 is comparatively low. With increasing current density, the energy-storing capacity decreases gradually, and the observed decrease is sharper for MNO7 than that for MNO4. The monotonic decline with the current density increase is typical of electrochemical double-layer supercapacitors.[48,60] The reduced values of C_{sp} at high current densities are associated with electrolytes' limited adsorption and desorption rates due to fast potential changes on the electrode material surface.[61] However, the highest C_{sp} is 627.9 F g^{-1} obtained with MNO7 nanoparticles at a current density of 0.1 mA cm^{-2}.

The obtained value of C_{sp} for MNO7 is much higher than some previously reported values for manganese dioxide systems, as summarized in Table 2, along with the comparison of the experimental and literature values of C_{sp}. It is clear that MNO7 with the highest C_{sp} (627.9 Fg^{-1}) is capable of storing more energy per unit mass than MNO4. This enhanced performance of MNO7 nanoparticles is associated with the increased permeation of the electrolyte ion's insight into the intergranular pores that resulted from the high-temperature treatment of the material, as can be visualized in the FESEM image (Figure 3). The high-temperature calcination of MNO7 results in a low aggregation of the nanoparticles, ensuring the high available surface area for electrolyte penetration (Figure 3). Such morphology of increased surface area will remarkably enhance the specific capacitance of MNO7. This increased interplanar space and accessible surface area allowed the active electrolyte ions (e.g., Na^+) to intercalate and deintercalate more efficiently and easily. It provided efficient ion transport pathways and a high charge storage capacity in the material. The accumulations of the manganese oxide particles of MNO4 result in a low surface area and narrow pores that limit the ion transfer required for efficient charging−discharging.[63,64] It was found that at low current density, the C_{sp} of MNO7 is higher, while at high current densities, this value is lower. This is because electrolyte ions permeate into electrode materials at low current density. The entire active electrode surface can store charge at low current density, which affects discharge time. At high current densities, diffusion hinders electrolyte ion migration, so only the outer active surface is used for charge storage. Thus, most nanostructured surfaces may not engage in electrochemical reactions due to kinetic considerations.[65−67]

The EIS carried out in a frequency range from 0.1 Hz to 1 MHz is shown in Figure 4c, and the relevant equivalent circuit is shown in the inset. The real axis provides quantitative information on the effective internal equivalent series resistances (ESRs) or the bulk resistance, R_s, at high frequencies, which is mainly related to uncompensated solution resistance, while the diameter of the semicircle indicates the charge-transfer resistance (R_{ct}). The R_s value of MNO7 and MNO4 is 6.92 and 28.48 Ω, respectively. The lowest R_s of MNO7 compared to that of MNO4 indicates that the electrical resistance of the active materials, electrolyte resistance, and contact resistance of MNO7 is low. Because the ESR is low, voltage drops at the start of a discharge curve may be very small for MNO7. This shows that MNO7 can act as a more highly conductive electrode material than MNO4. The values of R_{ct} are 3.77 and 4.99 Ω for MNO7 and MNO4, respectively, further verifying the difference in their structure and characteristics. Also, the vertical lines that appeared in the low-frequency region indicate the excellent capacitive behavior shown by MNO7 than by MNO4.[68,69]

The E and P of MNO4 and MNO7 electrode materials were calculated using eqs 2 and 3, respectively, and are depicted in the corresponding Ragone plot (Figure 5b). The calculated values are also summarized in Table 3. The MNO7 electrode material has a much higher E than the MNO4. However, the P values of both materials obtained at 400 and 700 °C were found to be almost equal (Table 3). For MNO7, the maximum E was 31.4 Wh kg^{-1} with a P of 100.0 W kg^{-1}. It maintains E of 0.49 Wh kg^{-1} at a high P of 803.5 W kg^{-1}, demonstrating excellent energy-power density behavior. The MNO4 electrode has a maximum E of only 5.66 Wh kg^{-1} at a P of 100.0 W $kg^{-1,}$ and the E decreased to 2.99 Wh kg^{-1} when the P increased to 803.3 W kg^{-1}. The good energy-power density behavior of the MNO7 resulted from the efficient ion diffusion process of the electrode material.[25] Having a high E usually corresponds to having a low P.[25] MNO7 with a good E (31.4 Wh kg^{-1}) and P (100.0 W kg^{-1}) will supply energy for a longer duration with a moderate rate of discharge of its stored energy. These results indicate that MNO7 could be the right electrode candidate for developing manganese oxide-based supercapacitors.

Study of Capacitance Retention. To demonstrate the performance of the electrochemical behavior of MNO7, a

https://doi.org/10.1021/acsomega.2c05872
ACS Omega 2022, 7, 48007−48017

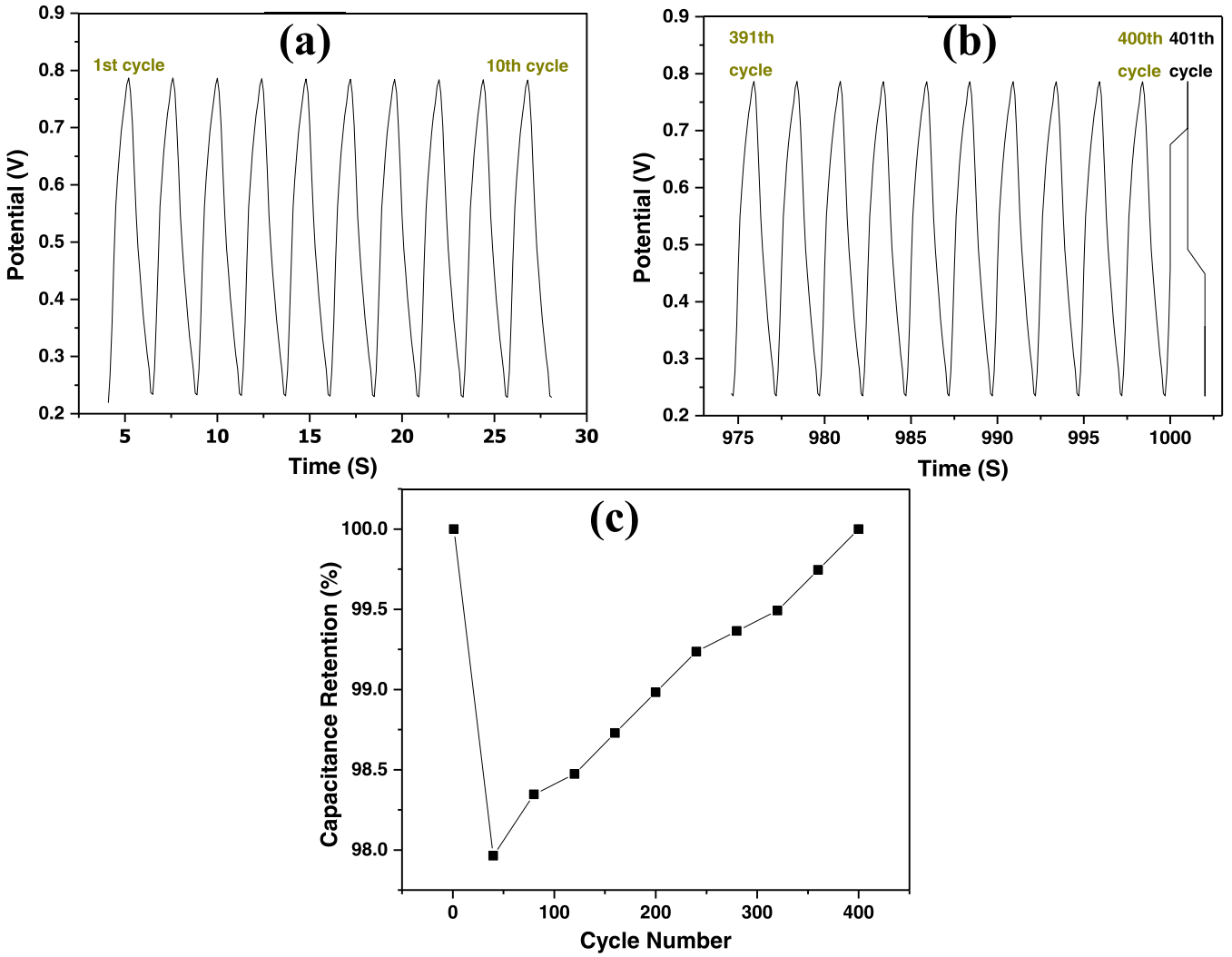

Figure 6. CD curves of MNO7 for (a) first and (a) last 10 cycles of the total 400 cycles along with the deformed 401st cycle within 0.2−0.8 V recorded by applying a current density of 1.0 mA cm^{-2} and (c) capacitance retention profile of MNO7.

charging−discharging cycle test was conducted with an electrochemical workstation at a current density of 1.0 mA $cm^{-2,}$ within the potential range of 0.2−0.8 V. The CD profile of the initial 10 cycles and the last 10 cycles of the total of 401 cycles are shown in Figure 6. The figures show that the CD curves have a typical triangular shape, even when charging and discharging for about 1000 s. It indicates the good electrochemical capacitive behavior of MNO7 nanoparticles. The CD curves exhibited an almost triangular shape up to 400 cycles shown. However, the 401st cycle deformed significantly. The values of C_{sp} were calculated from the CD profiles of 401 cycles with an interval of 40 cycles, which are presented in Figure SF5 (SI).

As represented in Figure 6c, a small drop in the capacitance retention (ca. 98%) during the first 40 cycles took place. However, a regain in the capacitance has been found to occur as the number of cycles increased. The decrease in the retention of capacitance with the number of cycles is common and is associated with the deactivation of the surface functionalities, detachment of active materials from the electrode surface,[57] stacking of material structure,[2,30] collapsing the pores and microstates, etc. The opposite explanations against the observation of the increment of capacitance have been usually given. In the present case, the lowering in capacitance that was found to regain eventually may occur for the lack of complete exposure of the active sites of the electrode surface to the electrolyte during repeated charging/discharging due to a slow wettability of the surface.[70]

CONCLUSIONS

Manganese oxide nanomaterials were successfully prepared using a gel formation technique, followed by calcination at 400 and 700 °C in an air atmosphere. The capacitive properties of electrode material were explored. Despite the different heat treatment temperatures, the materials were identified as MnO_2 in the EDX and XRD analyses. The prepared materials were in the nanodimension with a body-centered tetragonal lattice structure. The electrochemical performance evaluation revealed that the prepared materials had the ideal behavior of electrochemical capacitors with excellent cycling reversibility. The material that was heated at 700 °C had the highest C_{sp} (627.9 F g^{-1}), energy density (31.4 Wh kg^{-1}), and power density (803.5 W kg^{-1}) value and it was very stable when charged and discharged over and over again. This material, thus, could help make manganese oxide-based supercapacitors for practical application.

https://doi.org/10.1021/acsomega.2c05872
ACS Omega 2022, 7, 48007−48017

■ ASSOCIATED CONTENT

Supporting Information

The Supporting Information is available free of charge at https://pubs.acs.org/doi/10.1021/acsomega.2c05872.

Elemental analysis by EDX, thermal analysis: simultaneous TG/DTG/DTA curve, potential scan rate-dependent cyclic voltammograms, charging−discharging curves measured at different current densities, and electrochemical capacitive performance of the materials (PDF)

■ AUTHOR INFORMATION

Corresponding Authors

Md. Mominul Islam − *Department of Chemistry, University of Dhaka, Dhaka 1000, Bangladesh;* orcid.org/0000-0003-3896-6778; Email: mominul@du.ac.bd

Shakhawat H. Firoz − *Department of Chemistry, Bangladesh University of Engineering and Technology, Dhaka 1000, Bangladesh;* orcid.org/0000-0002-1771-462X; Email: shfiroz@chem.buet.ac.bd

Authors

Md. Abu Bakar Siddique − *Department of Chemistry, Bangladesh University of Engineering and Technology, Dhaka 1000, Bangladesh; Institute of National Analytical Research and Service, Bangladesh Council of Scientific and Industrial Research, Dhaka 1205, Bangladesh;* orcid.org/0000-0001-7947-1910

Ummey Hafsa Bithi − *Institute of Food Science and Technology, Bangladesh Council of Scientific and Industrial Research, Dhaka 1205, Bangladesh*

Aninda Nafis Ahmed − *Pilot Plant and Process Development Centre, Bangladesh Council of Scientific and Industrial Research, Dhaka 1205, Bangladesh*

M. A. Gafur − *Pilot Plant and Process Development Centre, Bangladesh Council of Scientific and Industrial Research, Dhaka 1205, Bangladesh*

Akter Hossain Reaz − *Department of Chemistry, Bangladesh University of Engineering and Technology, Dhaka 1000, Bangladesh;* orcid.org/0000-0001-9508-710X

Chanchal Kumar Roy − *Department of Chemistry, Bangladesh University of Engineering and Technology, Dhaka 1000, Bangladesh;* orcid.org/0000-0001-9894-3477

Complete contact information is available at: https://pubs.acs.org/10.1021/acsomega.2c05872

Author Contributions

M.A.B.S.: conceptualization, methodology, validation, formal analysis, investigation, data curation, writing—original draft preparation, writing—reviewing and editing, and visualization. U.H.B.: methodology, formal analysis, and investigation. A.N.A. and M.A.G.: validation, formal analysis, and investigation, A.H.R. and C.K.R.: writing—reviewing and editing. M.M.I.: methodology, resources, data curation, writing—reviewing and editing, and supervision. S.H.F.: conceptualization, methodology, resources, data curation, writing—reviewing and editing, and supervision. All authors read and approved the final manuscript.

Notes

The authors declare no competing financial interest.

■ ACKNOWLEDGMENTS

The authors are grateful to the Committee for Advanced Studies and Research (CASR), Bangladesh University of Engineering and Technology (BUET), for providing academic and technical support for this research work and necessary funds.

■ REFERENCES

(1) Huang, W.; Li, J.; Xu, Y. Nucleation and Growth of Porous MnO_2 Coatings Prepared on Nickel Foam and Evaluation of Their Electrochemical Performance. *Materials* **2018**, *11*, 716.

(2) Obeidat, A. M.; Gharaibeh, M. A. Electrochemical Performance of MnO_2 for Energy Storage Supercapacitors in Solid-State Design. *Int. J. Renewable Energy Res.* **2018**, *8*, 1229−1235.

(3) Deng, M. C. High-Performance, and Wearable Mn Oxide Supercapacitor with Urea-$LiClO_4$ Based Gel Electrolytes. *ACS Appl. Mater. Interfaces* **2017**, *9*, 479−486.

(4) Zhang, T.; Mao, Z.; Shi, X.; Jin, J.; He, B.; Wang, R.; Gong, Y.; Wang, H. Tissue-derived carbon microbelt paper: a high-initial-coulombic-efficiency and low-discharge-platform K^+-storage anode for 4.5 V hybrid capacitors. *Energy Environ. Sci.* **2022**, *15*, 158−168.

(5) Tarek, Y. A.; Shakil, R.; Reaz, A. H.; Roy, C. K.; Barai, H. R.; Firoz, S. H. Wrinkled Flower-Like rGO intercalated with Ni $(OH)_2$ and MnO_2 as High-Performing Supercapacitor Electrode. *ACS Omega* **2022**, *7*, 20145−20154.

(6) Reaz, A. H.; Saha, S.; Roy, C. K.; Wahab, M. A.; Will, G.; Amin, M. A.; Yamauchi, Y.; Liu, S.; Kaneti, Y. V.; Hossain, M.; Firoz, S. H. Boosting capacitive performance of manganese oxide nanorods by decorating with three-dimensional crushed graphene. *Nano Convergence* **2022**, *9*, No. 10.

(7) Islam, M. M.; Mollah, M. Y. A.; Susan, M. A. B. H.; Islam, M. M. Frontier performance of in situ formed α-MnO_2 dispersed over functionalized multi-walled carbon nanotubes covalently anchored to a graphene oxide nanosheet framework as supercapacitor materials. *RSC Adv.* **2020**, *10*, 44884−44891.

(8) Ali, G. A. M.; Tan, L. L.; Jose, R.; Yusoff, M. M.; Chong, K. F. Electrochemical performance studies of MnO_2 nanoflowers recovered from spent battery. *Mater. Res. Bull.* **2014**, *60*, 5−9.

(9) Song, J.; Li, H.; Li, S.; Zhu, H.; Ge, Y.; Wang, S.; Feng, X.; Liu, Y. Electrochemical synthesis of MnO_2 porous nanowires for flexible all-solid-state supercapacitor. *New J. Chem.* **2017**, *41*, 3750−3757.

(10) Edison, T. N. J. I.; Atchudan, T. N. R.; Atchudan, R.; Karthik, N.; Karthik, N.; Dangsheng, X.; Xiong, D.; Rok, L. Y. Direct electrosynthesis of MnO_2 nanoparticles over nickel foam from spent alkaline battery cathode and its supercapacitor performance. *J. Taiwan Inst. Chem. Eng.* **2019**, *97*, 414−423.

(11) Ali, G. A. M.; Yusoff, M. M.; Ng, Y. H.; Lim, H. N.; Chong, K. F. Potentiostatic and galvanostatic electrodeposition of manganese oxide for supercapacitor application: A comparison study. *Curr. Appl. Phys.* **2015**, *15*, 1143−1147.

(12) Liang, K.; Tang, X.; Hu, W. High-performance three-dimensional nanoporous NiO film as a supercapacitor electrode. *J. Mater. Chem.* **2012**, *22*, 11062−11067.

(13) Li, Y.; Liang, T.; Wang, R.; He, B.; Gong, Y.; Wang, H. Encapsulation of Fe_3O_4 between copper nanorod and thin TiO_2 film by ALD for lithium-ion capacitors. *ACS Appl. Mater. Interfaces* **2019**, *11*, 19115−19122.

(14) Salari, M.; Konstantinov, K.; Liu, H. K. 2011. Enhancement of the capacitance in TiO_2 nanotubes through controlled introduction of oxygen vacancies. *J. Mater. Chem.* **2012**, *21*, 5128−5133.

(15) Hossain, M. N.; Chen, S.; Chen, A. Fabrication and electrochemical study of ruthenium-ruthenium oxide/activated carbon nanocomposites for enhanced energy storage. *J. Alloys Compd.* **2018**, *751*, 138−147.

(16) Liu, Z.; Liang, F.; Zhang, N.; Liu, Y. Preparation of Manganese Dioxide/Polypyrol Composite by W/O Miniemulsion and Its Electrochemical Performance. *Int. J. Electrochem. Sci.* **2018**, *13*, 6584−6597.

(17) Zhang, J.; Zhao, X.; Huang, Z.; Xu, T.; Zhang, Q. High-Performance All-Solid-State Flexible Supercapacitors Based on Manganese Dioxide/Carbon Fibers. *Carbon* **2016**, *107*, 844−851.
(18) Yuan, L.; Wan, C.; Zhao, L. Facial In-situ Synthesis of MnO_2/PPy Composite for Supercapacitor. *Int. J. Electrochem. Sci.* **2015**, *10*, 9456−9465.
(19) Wei, W.; Cui, X.; Chen, W.; Ivey, D. Manganese Oxide-Based Materials as Electrochemical Supercapacitor Electrodes. *Chem. Soc. Rev.* **2011**, *40*, 1697−1721.
(20) Xi, S.; Zhu, Y.; Yang, Y.; Liu, Y. Direct Synthesis of MnO_2 Nanorods on Carbon Cloth as Flexible Supercapacitor Electrode. *J. Nanomater.* **2017**, *2017*, No. 7340961.
(21) Tang, X.; Li, H.; Liu, Z. H.; Yang, Z.; Wang, Z. Preparation and capacitive property of manganese oxide nanobelt bundles with birnessite-type structure. *J. Power Sources* **2011**, *196*, 855−859.
(22) Goikolea, E.; Daffos, B.; Taberna, P. L.; Simon, P. Synthesis of nanosized MnO_2 prepared by the polyol method and its application in high power supercapacitors. *Mater. Renewable Sustainable Energy.* **2013**, *2*, No. 16.
(23) Aghazadeh, M.; Maragheh, M. G.; Ganjali, M. R.; Norouzi, P.; Faridbod, F. Electrochemical preparation of MnO_2 nanobelts through pulse base-electrogeneration and evaluation of their electrochemical performance. *Appl. Surf. Sci.* **2016**, *364*, 141−147.
(24) Mishra, R. K.; Prajapati, C. S.; Shahi, R. R.; Kushwaha, A. K.; Sahay, P. P. Influence of electrodeposition modes on the electrochemical performance of MnO_2 films prepared using anionic $MnO_4^-(Mn^{7+})$ precursor. *Ceram. Int.* **2018**, *44*, 5710−5718.
(25) Wan, C.; Yuan, L.; Shen, H. Effects of Electrode Mass-loading on the Electrochemical Properties of Porous MnO_2 for Electrochemical Supercapacitor. *Int. J. Electrochem. Sci.* **2014**, *9*, 4024−4038.
(26) Radhiyah, A. A.; Izwan, M. I.; Baiju, V.; Feng, C. K.; Jamil, I.; Jose, R. Doubling of electrochemical parameters via the pre-intercalation of Na^+ in layered MnO_2 nanoflakes compared to α-MnO_2 nanorods,. *RSC Adv.* **2015**, *5*, 9667−9673.
(27) Su, D.; Ahn, H. J.; Wang, G. Hydrothermal synthesis of α-MnO_2 and β-MnO_2 nanorods as high capacity cathode materials for sodium ion batteries. *J. Mater. Chem. A* **2013**, *1*, 4845−4850.
(28) Yousefi, T.; Davarkhah, R.; Golikand, A. N.; Mashhadizadeh, M. H. Synthesis, characterization, and supercapacitor studies of manganese (IV) oxide nanowires. *Mater. Sci. Semicond. Process* **2013**, *16*, 868−876.
(29) Tizfahm, J.; Aghazadeh, M.; Mohammad, G. M.; Mohammad, R. Z.; Parviz, N.; Farnoush, F. Electrochemical preparation and evaluation of the supercapacitive performance of MnO_2 nanoworms. *Mater. Lett.* **2016**, *167*, 153−156.
(30) Yang, G.; Wang, B.; Guo, W.; Bu, Z.; Miao, C.; Xue, T.; Li, H. Liquid crystalline phase synthesis of nanoporous MnO_2 thin film arrays as an electrode material for electrochemical capacitors. *Mater. Res. Bull.* **2012**, *47*, 3120−3123.
(31) Yang, Y.; Huang, C. Effect of synthetical conditions, morphology, and crystallographic structure of MnO_2 on its electrochemical behavior. *J. Solid State Electrochem.* **2010**, *14*, 1293−1301.
(32) Yan, D.; Guo, Z.; Zhu, G.; Yu, Z.; Xu, H.; Yu, A. MnO_2 film with three-dimensional structure prepared by hydrothermal process for supercapacitor. *J. Power Sources* **2012**, *199*, 409−412.
(33) Wang, X.; Zheng, Y.; Xu, Z.; Wang, X.; Chen, X. Amorphous MnO_2 supported on carbon nanotubes as a superior catalyst for low temperature NO reduction with NH_3. *RSC Adv.* **2013**, *3*, 11539−11542.
(34) Wei, C.; Pang, H.; Zhang, B.; Lu, Q.; Lu, Q.; Liang, S.; Liang, S.; Gao, F. Two-dimensional β-MnO_2 nanowire network with enhanced electrochemical capacitance. *Sci. Rep.* **2013**, *3*, No. 2193.
(35) Duan, X.; Yang, J.; Gao, H.; Ma, J.; Jiao, L.; Zheng, W. Controllable hydrothermal synthesis of manganese dioxide nanostructures: shape evolution, growth mechanism and electrochemical properties. *CrystEngComm* **2012**, *14*, 4196−4204.
(36) Donne, S. W.; Hollenkamp, A. F.; Jones, B. C. Structure, morphology and electrochemical behaviour of manganese oxides prepared by controlled decomposition of permanganate. *J. Power Sources* **2010**, *195*, 367−373.
(37) Lin, C. K.; Chuang, K. H.; Lin, C. Y.; Tsay, C. Y.; Chen, C. Y. Manganese oxide films prepared by sol−gel process for supercapacitor application. *Surf. Coat. Technol.* **2007**, *202*, 1272−1276.
(38) Fan, X. Y.; Wang, X. L.; Li, G.; Yu, A. P.; Chen, Z. W. High-performance flexible electrode based on electrodeposition of polypyrrole/MnO_2 on carbon cloth for supercapacitors. *J. Power Sources* **2016**, *326*, 357−364.
(39) Ming, B.; Li, J.; Kang, F.; Pang, G.; Zhang, Y.; Chen, L.; Xu, J.; Wang, X. Microwave−hydrothermal synthesis of birnessite-type MnO_2 nanospheres as supercapacitor electrode materials. *J. Power Sources* **2012**, *198*, 428−431.
(40) Ullah, A. K. M. A.; Kibria, K. M. F.; Akter, M.; Khan, M. N. I.; Maksud, M. A.; Jahan, R. A.; Firoz, S. H. Synthesis of Mn_3O_4 nanoparticles via a facile gel formation route and study of its phase and structural transformation with distinct surface morphology upon heat treatment. *J. Saudi Chem. Soc.* **2017**, *21*, 830−836.
(41) Dhaouadi, H.; Ghodbane, O.; Hosni, F.; Touati, F. Mn_3O_4 nanoparticles: synthesis, characterization, and dielectric properties. *ISRN Spectrosc.* **2012**, *2012*, No. 706398.
(42) Sarkar, A.; Singh, A. K.; Sarkar, D.; Khan, G. G.; Mandal, K. Three-Dimensional Nanoarchitecture of $BiFeO_3$ Anchored TiO_2 Nanotube Arrays for Electrochemical Energy Storage and Solar Energy Conversion. *ACS Sustainable Chem. Eng.* **2015**, *3*, 2254−2263.
(43) Lee, J. W.; Hall, A. S.; Jong-Duk Kim, J. D.; Mallouk, T. E. A Facile and Template-Free Hydrothermal Synthesis of Mn_3O_4 Nanorods on Graphene Sheets for Supercapacitor Electrodes with Long Cycle Stability. *Chem. Mater.* **2012**, *24*, 1158−1164.
(44) Wang, J.*Analytical Electrochemistry*; John Wiley and Sons Ltd. Inc.: New York, 2000.
(45) Conway, B. E.*Electrochemical Supercapacitors*; Kluwer Academic Publishers: New York,1999.
(46) Zhao, D.; Guo, X.; Gao, Y.; Gao, F. An electrochemical capacitor electrode based on porous carbon spheres hybrided with polyaniline and nanoscale ruthenium oxide. *ACS Appl. Mater. Interfaces* **2012**, *4*, 5583−5589.
(47) Deng, L.; Wang, J.; Zhu, G.; Kang, L.; Hao, Z.; Lei, Z.; Yang, Z.; Liu, Z. H. **2014**, RuO_2/graphene hybrid material for high performance electrochemical capacitor. *J. Power Sources* **2012**, *248*, 407−415.
(48) Li, Z. P.; Wang, J. Q.; Liu, X. H.; Liu, S.; Ou, J. F.; Yang, S. R. Electrostatic layer-by- layer self-assembly multilayer films based on graphene and manganese dioxide sheets as novel electrode materials for supercapacitors. *J. Mater. Chem.* **2011**, *21*, 3397−3403.
(49) Zhao, J.; Li, Y.; Chen, X.; Zhang, H.; Song, C.; Liu, Z.; Zhu, K.; Cheng, K.; Ye, K.; Yan, J.; Cao, D.; et al. Polyaniline-modified porous carbon tube bundles composite for high-performance asymmetric supercapacitors. *Electrochim. Acta* **2018**, *292*, 458−467.
(50) Zhang, J.; Jiang, J.; Zhao, X. S. Synthesis and Capacitive Properties of Manganese Oxide Nanosheets Dispersed on Functionalized Graphene Sheets. *J. Phys. Chem. C* **2011**, *115*, 6448−6454.
(51) Terayama, K.; Ikeda, M. Study on Thermal Decomposition of MnO_2 and Mn_2O_3 by Thermal Analysis. *Trans. Jpn. Inst. Met.* **1983**, *24*, 754−758.
(52) Agrawal, R. D. Simultaneous TG, DTG and DTA studies on Manganese Oxides. *Trans. Jpn. Inst. Met.* **1981**, *22*, 253−257.
(53) Jaganyi, D.; Altaf, M.; Wekesa, I. Synthesis and characterization of whisker-shaped MnO_2 nanostructure at room temperature. *Appl. Nanosci.* **2013**, *3*, 329−333.
(54) Yang, Z.; Xia, G.; Stevenson, J. W. $Mn_{1.5}Co_{1.5}O_4$ spinel protection layers on ferritic stainless steels for SOFC interconnect applications. *Electrochem. Solid-State Lett.* **2005**, *8*, A168.
(55) Yang, X.; Makita, Y.; Liu, Zh.; Sakane, K.; Ooi, K. Structural Characterization of Self-Assembled MnO_2 Nanosheets from Birnessite Manganese Oxide Single Crystals. *Chem. Mater.* **2004**, *16*, 5581.
(56) Rui, D.; Kun-De, Y.; Yuan-Liang, M.; Bo, L. A reliable acoustic path: Physical properties and a source localization method. *Chin. Phys. B* **2012**, *21*, No. 124301.

https://doi.org/10.1021/acsomega.2c05872
ACS Omega 2022, 7, 48007−48017

(57) Sourav, S.; Tapas, K. G.; Dipak, R.; Indranil, R.; Amartya, B.; Gunjan, S.; Mukut, C.; Dipankar, C. Studies on synthesis of reduced graphene oxide (rGO) via green route and its electrical property. **2015**. *Mater. Res. Bull.* **2015**, *63*, 80−87.
(58) Askar, M.; Abbas, H. Chemically activated manganese dioxide for dry batteries. *J. Power Sources* **1994**, *51*, 319−330.
(59) Reddy, R. N.; Reddy, R. G. Sol-gel MnO_2 as an electrode material for electrochemical capacitors. *J. Power Sources* **2003**, *124*, 330−337.
(60) Karthikeyan, K.; Kalpana, D.; Amaresh, S.; Lee, Y. S. Microwave synthesis of graphene/magnetite composite electrode material for symmetric supercapacitor with superior rate performance. *RSC Adv.* **2012**, *2*, 12322−12328.
(61) Hu, Z.; Zu, L.; Jiang, Y.; Lian, H.; Liu, Y.; Li, Z.; Chen, F.; Wang, X.; Cui, X. High specific capacitance of polyaniline/mesoporous manganese dioxide composite using KI-H_2SO_4 electrolyte. *Polymers* **2015**, *7*, 1939−1953.
(62) Edison, T. N. J. I.; Atchudan, R.; Karthik, N.; Xiong, D.; Lee, Y. R. Direct electro-synthesis of MnO_2 nanoparticles over nickel foam from spent alkaline battery cathode and its supercapacitor performance. *J. Taiwan Inst. Chem. Eng.* **2019**, *97*, 414−423.
(63) Zhou, Z.; Zhu, Y.; Wu, Z.; Lu, F.; Jing, M.; Ji, X. Amorphous RuO_2 coated on carbon spheres as excellent electrode materials for supercapacitors. *RSC Adv.* **2014**, *4*, 6927−6932.
(64) Zhang, C.; Xie, Y.; Zhao, M.; Pentecost, A. E.; Ling, Z.; Wang, J.; Long, D.; Ling, L.; Qiao, W. Enhanced electrochemical performance of hydrous RuO_2/mesoporous carbon nanocomposites via nitrogen doping. *ACS Appl. Mater. Interfaces* **2014**, *6*, 9751−9759.
(65) Shaheen Shah, S.; Abu Nayem, S. M.; Sultana, N.; Saleh Ahammad, A. J.; Abdul Aziz, M. Preparation of Sulfur-doped Carbon for Supercapacitor Applications: A Review. *ChemSusChem* **2022**, *15*, No. e202101282.
(66) Shah, S. S.; Cevik, E.; Aziz, M. A.; Qahtan, T. F.; Bozkurt, A.; Yamani, Z. H. Jute sticks derived and commercially available activated carbons for symmetric supercapacitors with bio-electrolyte: a comparative study. *Synth. Met.* **2021**, *277*, No. 116765.
(67) Ratajczak, P.; Suss, M. E.; Kaasik, F.; Béguin, F. Carbon electrodes for capacitive technologies. *Energy Storage Mater.* **2019**, *16*, 126−145.
(68) Wang, X.; Chen, L.; Zhang, S.; Chen, X.; Li, Y.; Liu, J.; Lu, F.; Tang, Y. Compounding δ-MnO_2 with modified graphene nanosheets for highly stable asymmetric supercapacitors. *Colloids Surf., A* **2019**, *573*, 57−66.
(69) Fang, C.; Zhang, D. A large areal capacitance structural supercapacitor with a 3D rGO@ MnO 2 foam electrode and polyacrylic acid−Portland cement−KOH electrolyte. *J. Mater. Chem. A* **2020**, *8*, 12586−12593.
(70) Wimalasiri, Y.; Fan, R.; Zhao, X. S.; Zou, L. Assembly of Ni-Al layered double hydroxide and graphene electrodes for supercapacitors. *Electrochim. Acta* **2014**, *134*, 127−135.

https://doi.org/10.1021/acsomega.2c05872
ACS Omega 2022, 7, 48007−48017